scientific reports

Check for updates

OPEN

A novel fully biobased material composite for cosmetic packaging applications

Fátima Santos[1,2]✉, Pedro Rodrigues[3], Patrício Vargas[4], Anabela Massano[4], Luís Miguel Oliveira[5], Catarina Batista[4], Vasco Cruz[3], Artur Mateus[4,6], Geoffrey R. Mitchell[4,7], Abílio J. F. N. Sobral[2] & Telma Encarnação[1,2]✉

The extensive production and use of fossil-based plastics have led to their ubiquity worldwide, causing growing concern and environmental problems. Consequently, developing biobased polymers and biobased composite materials, aligned with circular economy principles, is now the focus as a sustainable alternative to fossil-based plastics. This work aimed to develop and characterise a new, fully biobased, and biodegradable material composite with properties similar to traditional fossil-based plastics, allowing its use in cosmetic product applications as an alternative to commonly used fossil-based plastics. A novel biobased composite comprising poly(3-hydroxybutyrate-co-3-hydroxyvalerate (PHBV), polylactic acid (PLA) chitosan (CS), acetyl tributyl citrate (ATBC) plant essential oils, and phycocyanin was successfully developed and processed using various techniques confirming its processability and versatility. Characterisation of the developed composites showed a reduction in mechanical properties with the addition of ATBC, essential oil and phycocyanin, with tensile results within the typical behaviour for PP (polypropylene) and PE (polyethylene). The thermal properties of the developed composites showed working temperatures in the same range as PP and PE. The results obtained are promising and, to the best of our knowledge, this work presents the first green material composite comprising PHBV, PLA, CS, essential oil, ATBC, and phycocyanin specifically designed for cosmetic packaging as a sustainable alternative to fossil-based plastics.

Keywords Biobased polymers, Biocomposites, PHBV, PLA, Additive manufacturing, Cosmetic packaging

Fossil-based plastics are widely manufactured and used by plastic industries, and their global consumption has been increasing over the years[1,2]. The estimated world plastic production in 2023 was around 374 million tons, of which 54 million tons were produced in Europe[3]. Owing to its properties of resilience, lightweightness, cost effectiveness, and durability, some estimates expect the amount of plastic production to triple by 2050[2,4,5]. Plastic production for packaging solutions accounts for approximately 36% of the total plastic production[6], even though plastic products are predominantly discharged after one single use.

Although many breakthroughs have been made, conventional plastic uses are currently associated with a series of disadvantages and problems, such as worsening the global warming problem, the nonbiodegradability of the majority of petroleum-based plastics, public health risks and the environmental concerns associated with these plastics due to pollution and biodiversity loss[2,5–7]. The main strategy used to address plastic waste in Europe is first energy recovery (heat, electricity, and fuel through incineration, among other processes) and second recycling[8]. Low recycling rates are reported in the literature: a study reported that only 7% of plastic is globally recycled[2]; in the United States, 5% of plastics were recycled in 2022 according to Greenpeace, with a declining tendency observed in recent years[9]; specifically, for packaging plastic, the recycling rates are estimated to be approximately 14% globally[10]. Moreover, plastic production is increasing[5], and polyethylene (PE) and polypropylene (PP) are the most common polymers of fossil-based use in several applications[11,12]. Cosmetic and detergent packaging solutions are produced mainly from PE, and PP is used in many subsegments in rigid

[1]PTScience, Alcobaça 2460-060, Portugal. [2]Coimbra Chemistry Centre-Institute of Molecular Sciences (CQC-IMS), Department of Chemistry, University of Coimbra, Coimbra 3004-535, Portugal. [3]IPC, University of Minho, Campus de Gualtar, Guimarães 4800-058, Portugal. [4]Centre for Rapid and Sustainable Product Development (CDRSP), Polytechnic Institute of Leiria, Marinha Grande 2430-028, Portugal. [5]AMCubed Lda, Rua Barão de Viamonte 18, 2410-020 Andrinos, Leiria, Portugal. [6]Instituto para a Sustentabilidade e Inovação em Estruturas de Engenharia (ISISE), Departamento de Engenharia Civil, Coimbra, Portugal. [7]Visionary Equation Unipessoal Lda, Rua do Sobreiro nº 38, Marinha Grande, Portugal. ✉email: fatima.santos@ptscience.pt; tencarnacao@qui.uc.pt

and flexible solutions[13,14]. The global cosmetic packaging market has been growing and is expected to reach 51 billion euros in 2032[15]. Soils, rivers, and oceans acted as sinks for an estimated 22 million tons of plastic in 2019, and this value is expected to double by 2060[8]. The extensive production and applications of plastics have led to their global widespread distribution resulted in political awareness and the need to develop new sustainable alternatives to petroleum-based plastics[2,10,16]. Biobased and biodegradable alternatives to fossil-based plastics need to be developed and adopted. The development of biobased polymers and biobased material composites as alternatives to fossil-based plastics for use in product applications can be part of the solution[4,5,10,16,17]. This approach follows circular economy principles and has been increasing: the global production of bioplastics is expected to increase from 2.18 million tons in 2023 to approximately 7.43 million tons in 2028[18]. Compared with fossil-based plastics, biobased plastics (from biological or human-made sources) have several advantages: (a) they have similar physicochemical properties; (b) they are renewable and biodegradable; (c) they have a smaller carbon footprint and fewer health risks; and (d) they mitigate environmental concerns and promote changes in consumer preferences[5,10]. The polymers used in this investigation were chosen because they have the above described characteristics/properties. The other constituents were selected because of their availability and cost-effectiveness. Despite the advantages of using biobased plastics, these are not free from associated challenges: high costs, reduced production efficiency at a small scale and even incompatibility with production and recycling processing that already exist[19].

Polylactic acid (PLA) (Fig. 1a) is a thermoplastic and a biodegradable biobased aliphatic polyester produced from natural resources[20,21]; moreover, it is one of the most commonly used and optimized polymers for product applications[20–22]. PLA is one of the main biopolymers and is considered suitable for replacing materials of petroleum-based plastics[17]; it has optical, thermal, mechanical, and barrier properties comparable with those of fossil-based plastics and shows potential for use in highly innovative products[20,21,23]. This biopolymer has good integral properties, mechanical processing, and high strength but poor rigidity[20,22]. To enhance the properties of biopolymers and ultimately their performance in product applications, they can be blended with other biodegradable polymers or other inorganic fillers[24]. The blending of poly(3-hydroxybutyrate-co-3-hydroxyvalerate) (PHBV) (Fig. 1b) with PLA has been extensively studied and reported in the literature for packaging solutions[12] where with increasing PLA concentrations, the properties are enhanced[25]. The thermal stability and flammability resistance are improved in the PHBV/PLA blends, their properties are improved, and processing is facilitated[25,26]. PHBV belongs to the family of polyhydroxyalkanoates (PHAs) and is produced by microorganisms capable of using different carbon substrates as sources[27–29]. This biobased polymer is usually hydrophobic, moisture resistant and water insoluble[30]. The Young's modulus (3–6 GPa), tensile strength (22–34 MPa), melting temperature, crystallinity, glass transition, and temperature of PHBV are comparable to those of PP and PE[7,24,28,29,31], which are very common petroleum-based polymers used for plastic production. Chitosan (CS) (Fig. 1c) can be used as a reinforcement for biobased material composites and has a positive impact on the environment through waste material usage and valorisation. It is the second most abundant polymer[32], and millions of tons are extracted annually from diverse sources[33,34]. CS is available and inexpensive, has high crystallinity and degradability, is water soluble, and allows for chemical changes[33–39]; thus, it is a good reinforcement polymer for incorporation in material composites that can be used as a substitute for fossil-based plastics. Some difficulties associated with the addition of CS to material composites include poor mechanical properties and poor solubility at physiological pH (7.4)[33,34]. Another component that can be added to a material composite to enhance material properties is plant essential oils (EOs); these are composed mainly of monoterpenes such as limonene or eucalyptol (Fig. 1f). EOs are widely used along with biopolymers, especially

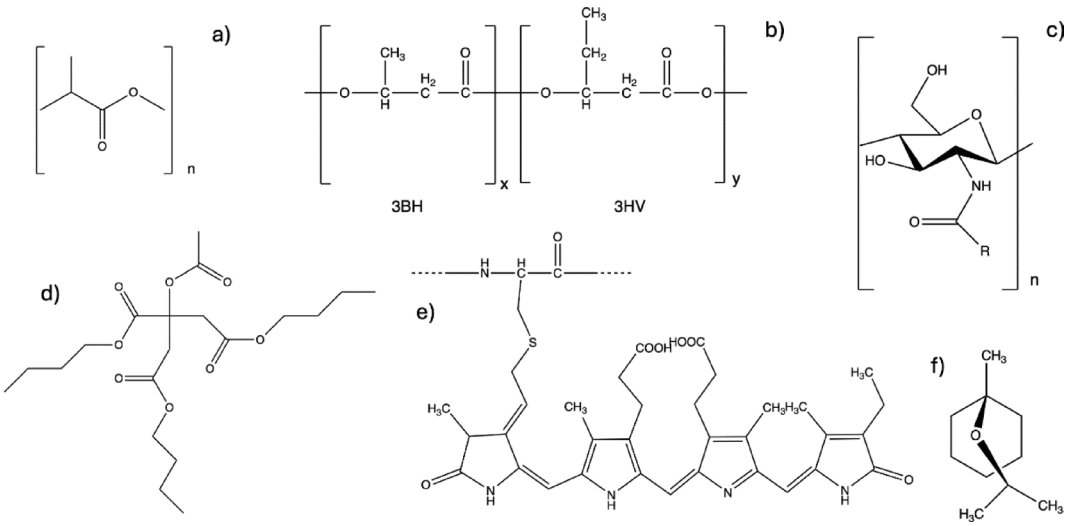

Fig. 1. Chemical structures of the biomaterials used in the formulation of the selected composite. (**a**) Polylactic acid (PLA); (**b**) poly(3-hydroxybutyrate-co-3-hydroxyvalerate) (PHBV); (**c**) N-acetylated chitosan (CS); (**d**) Acetyl tributyl citrate (ATBC); (**e**) phycocyanin (Pgm); (**f**) eucalyptol (representative molecule of the plant oil used) (EO).

in the food industry[40–43]. The incorporation of essential oils in biobased material composites can decrease the water vapour permeability[44]. A study reporting the incorporation of essential oils into CS-based film-forming dispersions and edible films confirmed that composite films containing EOs were less rigid, more stretchable, and softer than composites free of EOs[45]. Additionally, essential oils can impart a fragrance/aroma to the developed material, increasing its value for cosmetic applications. Although EOs are natural compounds, they can interfere with the human endocrine system; however, they still cause potentially less harm than persistent synthetic compounds.

Considering its application in cosmetic packaging, the addition of a natural colorant such as phycocyanin (Fig. 1e), which has an intense and appealing blue colour[46,47], can increase its packaging value[47,48]. Moreover, the selection of phycocyanin can help to show whether natural pigments are a viable option for replacing synthetic colouring molecules while also considering the processing temperature profile (bioactive compound degradation temperature-colour change and loss). Citrate in the form of acetyl tributyl citrate (ATBC) (Fig. 1d), was also used in the development of the material composites described in this work. ATBC has been thoroughly studied and is widely used as effective plasticizer for PLA[49–52]. The use of ATBC along with PLA increases ductility, processability, and flexibility and reduces inherent brittleness through the introduction of rubber particles that improve the impact properties and elongation at break[49–51,53]. By adding ATBC to PLA, the glass transition temperature (*Tg*) is reduced, and the crystallization rate is improved[49]; however, ATBC can also be responsible for the strength and modulus loss of PLA[50]. For this associated problem, reinforcements (such as CS) can be a good solution. Here, ATBC was selected for different reasons: (a) its physical-chemical properties dictate its miscibility with the biopolymers chosen, (b) it has a limited impact in the environment; and (c) ATBC is biodegradable, biocompatible (nontoxic), biobased and environmentally friendly[49,50,53]. In addition, the additive manufacturing (AM) process can be improved because all constituents in the developed formulation have very distinct melting temperatures, which cause a challenge to the process.

Considering the disadvantages associated with fossil-based plastics and the previously described challenges, the aim of this work is to develop a new material composite that is fully biobased and biodegradable and created with cost-effective and available constituents for applications in cosmetic packaging.

Results and discussion

The developed formulations were evaluated in terms of their characteristics. The structure (FTIR and XRD), topography (SEM analysis), thermal behaviour (TGA and DSC), rheological characteristics (MFR), mechanical properties (tensile tests) and hydrophobicity (WCA) of the developed material composites were examined.

The chemical structure of the formulations described in this work was evaluated using FTIR. Figure 2 shows the FTIR spectra for PLA, PHBV, PHBV/PLA, PHBV/PLA/CS and PHBV/PLA/CS/Pgm/OE/ATBC. The absorption bands for PLA showed the characteristic behaviour of this polymer reported in other literature publications: C–H stretching in the approximate region of 2900 cm^{-1} (2985, 2915, 2847 cm^{-1}), C = O stretching of polyesters in the region of 1746 cm^{-1}, $-CH_3$ asymmetric bending at 1449 cm^{-1}, C–O–C stretching bands in the region of 1081 cm^{-1} and 1078 cm^{-1}[54]. The absorption bands for PHBV were as follows: the C-H stretching band at 2968 and 2913 cm^{-1}, C = O stretching at 1720 cm^{-1} and O-H bending in the region of 1400 cm^{-1} (1377 cm^{-1} and 1440 cm^{-1})[55,56]. The other evaluated formulations showed similar peaks as those of the polymers (PLA and

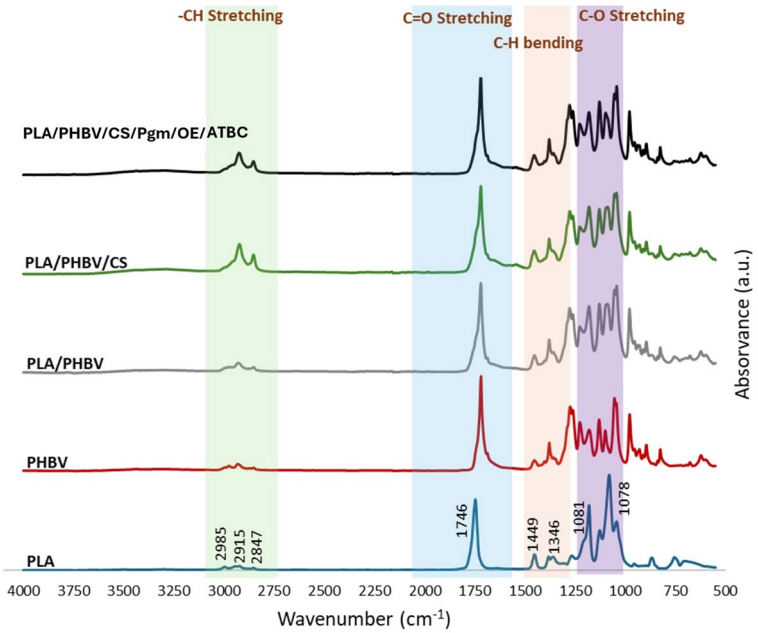

Fig. 2. FTIR spectra of the developed formulations: PLA, PHBV, PHBV/PLA, PHBV/PLA/CS and PHBV/PLA/CS/OE/Pgm/ATBC.

PHBV); these results potentially indicated that no new or strong chemical interactions were formed within the formulation components. The intensity of the C = O stretching peak of the formulation PHBV/PLA was lower than the intensity of PLA or PHBV alone; these results indicated a loss of carboxylic groups in this formulation[55].

Each of the injection moulded specimens prepared from the series of materials listed in Table 7 were subjected to X-ray scattering measurements at room temperature. The moulded sample was mounted on a translation stage, which enabled measurements at three equidistant points along the centre line of the long axis of the sample. The small-angle X-ray scattering data were recorded simultaneously with the wide-angle X-ray scattering data. The primary data were displayed as a false colour image of the intensity recorded on the pixelated detector. The long axis of the detector corresponded to the scattering angle of 2θ, whereas the azimuthal variation corresponded to the arc bands of intensity. The mapping of colour to intensity was shown in the colour map situated next to the intensity map. Fig. S1 (Supplementary Information) shows an image recorded at the first position for the PLA sample. The accompanying line plot showed the azimuthual average of the points with an equivalent value of $|Q|$. The image showed numerous diffuse peaks at $|Q|$ values of 10.58, 21.69 and 51.85 nm^{-1}. These diffuse peaks were typical in X-ray scattering curves of polymers in the amorphous state[57,58]. The most intense peak at $|Q| \sim 10.6$ nm^{-1} originated from the short-range correlations between neighbouring chain segments, and the width of this peak at half of the maximum intensity of 7.94 nm^{-1} resulted in a correlation length of ~ 0.8 nm. Figure 3 shows a continuous scattering curve; here, the diffuse peaks corresponded to an amorphous polymer. No sharp crystalline peaks were observed at a scattering vector of ~ 11 nm^{-1}; this was the position of the (200) crystal reflection for the α phase of PLA. Previous studies reported that PLA was a slow crystallizer and that the crystal structures of crystals formed at high and low temperatures were different[59,60]. The curve in Fig. 3 showed no evidence of sharp crystalline reflections of either crystal structure. The data recorded at the three positions within the injection moulded part were more or less identical to those shown here, and we only showed the data from one sampling position. Inspection of the azimuthal variation in peak intensity reveals a more or less constant intensity, indicating the absence of any preferred orientation. For completeness, the SAXS pattern for the same sample and sampling point is shown in Fig. 3. Fig. S2 (Supplementary Information) also shows a false colour image of the scattering data. This result showed minimal small-angle X-ray scattering except close to the zero-angle position and indicated a high level of homogeneity, which would be typical for most amorphous polymers. An intensity streak was vertically observed through the zero-angle position and indicated a small presence of extended objects that ran parallel to the flow direction in the moulded part. We attributed this streak to the extension of nanovoids in the moulded part, which were extended by the injection moulding process in the direction of flow. Fig. S3 (Supplementary Information) shows the equivalent data for the PHBV moulded part. The false colour image shown in Fig. S3 (Supplementary Information) displayed a series of sharp arcs of intensity typical of a semicrystalline state. These could be clearly observed in the accompanying line plot shown in Fig. 4. Table 1 shows the positions of the first 10 sharp peaks in the pattern.

Compared with other reported studies on PHBV using X-ray scattering, similar results were attained for PHBV polymers with low HV contents[61]. From the curve in Fig. 4, we could estimate that the level of crystallinity was relatively high. Fig. S4 (Supplementary Information) shows a ring of uniform intensity almost at the physical edge of the detector. In the centre of the patterns, some scattering around the beam is typically observed in a semicrystalline polymer. The horizontal streak was attributed to the presence of nanovoids, as in the PLA sample. This peak was at the limit of what could be measured, but we could estimate the position of this peak at $|Q| \sim 1.3$ nm^{-1}; this resulted in a long period (the chain-fold crystal thickness plus the amorphous material between crystals) of 4.83 nm. Due to the isotropic nature of the intensity distribution in this ring, no preferential alignment of the chain-folded lamellar crystals occurred. Fig. S5 (Supplementary Information) shows false colour intensity maps of the wide-angle X-ray scattering results for the mixtures of PLA and PHBV listed in

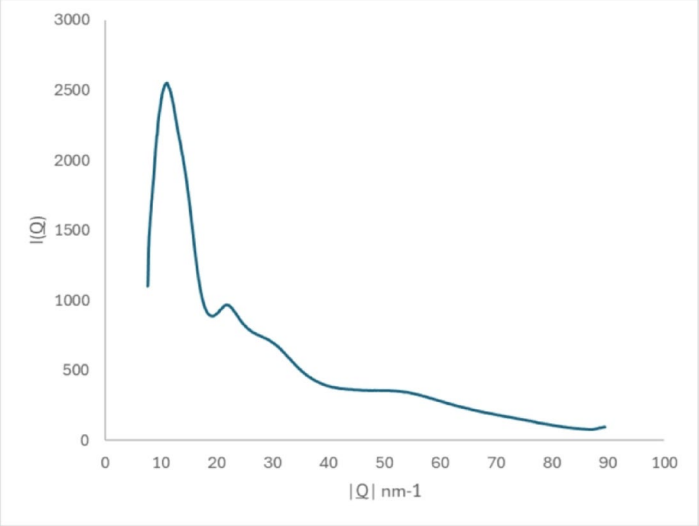

Fig. 3. The azimuthal average for the data shown in Figure S1.

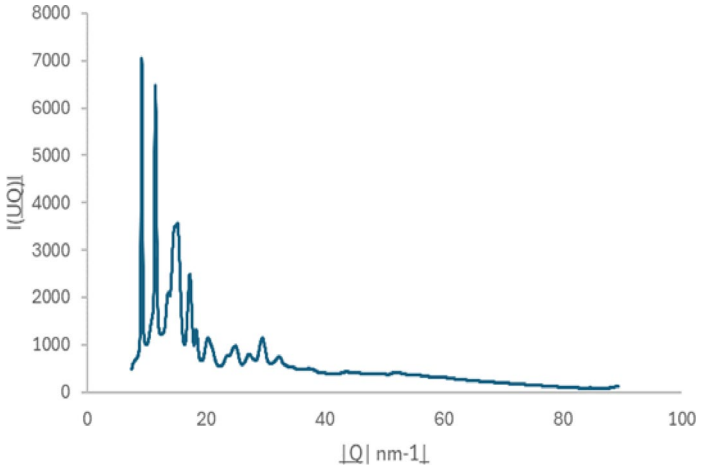

Fig. 4. The azimuthual averaged WAXS data for the injection moulded parts fabricated from PHBV.

Peak	Position (nm^{-1})	Intensity	Notes
1	8.79	vs.	
2	11.26	vs.	
3	13.74	s	Shoulder
4	14.84	s	Overlapping peaks
5	17.03	s	
6	18.13	w	
7	20.33	w	
8	24.73	w	
9	26.92	w	
10	29.12	w	

Table 1. Positions of the first 10 peaks observed in the pattern for PHBV. vs. – very strong, s – strong, w – weak.

Table 1. The patterns were broadly similar to those shown for the PHBV samples but with small variations in the sharp peaks in each pattern; these results reflected the differences in composition, as shown in Table 1. The crystal reflections again showed a uniform variation in intensity as a function of the azimuth angle, indicating an isotropic distribution of crystals in these samples. The three curves shown in Fig. 5 were very similar to the intensity plot for the PHBV shown in Fig. 4 in terms of peak position, peak width and relative peak intensity. These results indicated that in these mixtures, the PHBV crystallised with a similar crystal structure as in the single-component system in Fig. 4. The PLA and citrate components did not crystallise. These components were incorporated into the amorphous phase of the PHBV, which had a greater presence in the scattering curves moving from the simple mixture to the 5-component system. Fig. S6 (Supplementary Information) shows the SAXS patterns for the samples studied in Fig. 4. All three patterns had similar features: lamellar stack scattering showed some small variation in peak position, and S7c showed much stronger scattering around the zero-angle position, reflecting a high level of heterogeneity. These results indicated that the multiple components were not incorporated into a single disordered phase but were present as distributed nanoscale phases. All three samples showed an isotropic distribution of chain-folded lamellar crystals. None of the three samples exhibited a streak of scattering around the zero-angle position, which was attributed to previous samples associated with nanovoids. In all cases, the three sampling points along the long length of the moulded part yielded essentially equivalent SAXS and WAXS data; these results confirmed the nonuniformity of the structure and morphology of the moulded parts. For all the moulded parts, the orientation of the crystals exhibited an isotropic orientation distribution.

SEM analysis was carried out on the cross-sections of the composite materials developed and on the neat polymers to analyse the morphology and distribution of the components that constitute the materials. For neat PLA (Fig. 6a), a flat surface was observed and indicated brittle fracture at the location of rupture. This was reported as a typical fracture surface for amorphous polymers where no visible plastic deformation was observed[26]. PHBV (Fig. 6b) showed a rupture surface different from that of neat PLA. The irregular fracture surface was attributed to the crystalline structure of PHBV and its more ductile fracture behaviour. In the PHBV/PLA formulation, a relatively smooth surface was observed with two distinctive phases, indicating the poor miscibility of the PHBV and PLA polymers at these weight ratios[25,26]. Figure 6c) shows a transition from

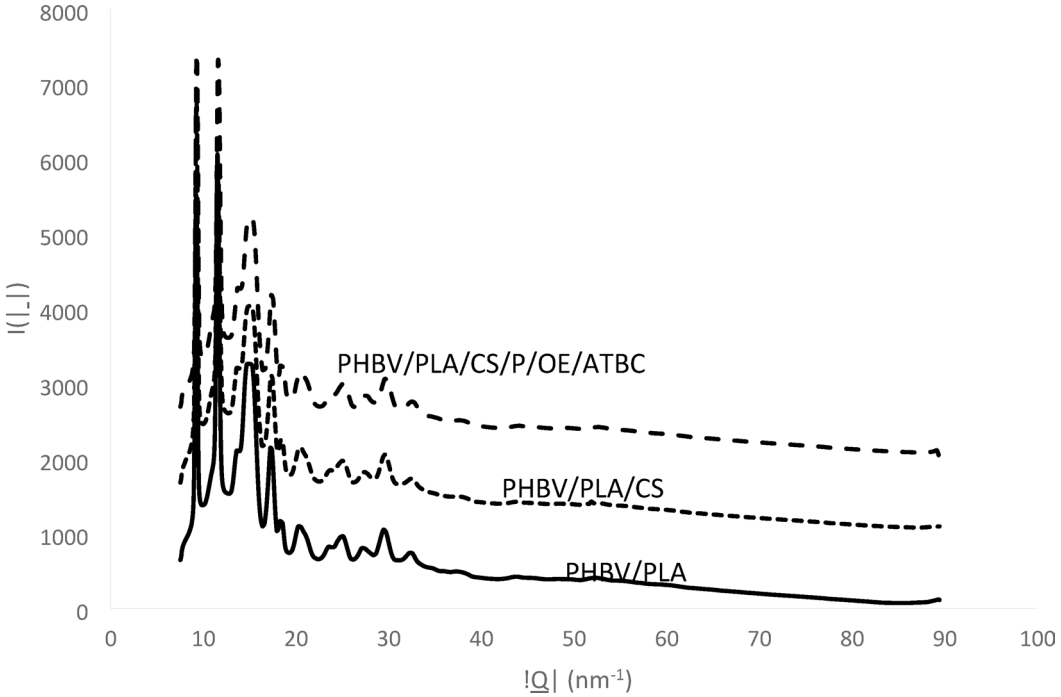

Fig. 5. Plots of the azimuthual averaged Intensity calculated from the intensity maps shown in Figure S5 (Supplementary Information).

a continuous phase to a droplet-matrix type with the existence of interpenetrating structures; here, small PLA droplets were dispersed in the PHBV matrix and regions where the two phases coexisted. Additionally, cavities were observed around the PLA droplets and indicated weak interfacial interactions between the two polymers (helping justify the fracture at this specific point). As shown in Fig. 6d), the morphology of the PHBV/PLA/CS formulation was similar to that of the previously described formulation: two phases coexisted in the matrix with visible cavities and holes; this result was expected based on the similarities between this formulation and the previously described formulation (the difference is the addition of CS). The red circles in the image outline the incorporation of the CS fibres. Additionally, the red rectangle represents the place where a CS fibre is pulled off. With respect to the most complex formulation developed (Fig. 6e), visual differences with respect to those previously described were observed. Fewer cavities and holes were observed and potentially indicated a more compact composition and increased flexibility because ATBC affected the crystallization during heating by increasing chain mobility. This result was not observed in the mechanical testing, since the Young's modulus for this formulation did not increase (compared with those of the other formulations). Even though fewer cavities and holes are visible in this formulation they are still visible indicating weak interfacial interactions[26]. The visual differences were also related to the addition of essential oil (OE) and pigment (Pgm), which we hypothesize were mostly degraded during the heating (injection) process.

The thermal stability/degradation of PLA, PHBV and the blends developed were investigated in terms of weight loss (%) by thermogravimetric analysis carried out under a nitrogen atmosphere. Knowledge of the thermal stability and properties of narrow processing materials is very important, especially for composite production due to the effect of fillers on the thermal behaviour of the material. During the heating process, the initial degradation temperature was marked when the sample weight decreased by 2% (T_2). Another important thermal property was obtained using derivative thermogravimetric (DTG) curves (Fig. 7, right); here, the temperature corresponding to the maximum rate of weight loss (T_p) was defined as the peak value of the first derivative of the TGA curve and provided a good indication of the temperature at which the maximum weight loss was triggered. The T_2 and T_p values are summarized in Table 2. PLA had the highest thermal stability, with an initial degradation temperature of 308 °C. For PHBV and the other blends, thermal degradation began earlier (255–262 °C); thus, PHBV and the other developed blends had similar thermal stabilities but lower thermal stabilities than those of the neat PLA. Similar results are reported in the literature, considering that the thermal stability is mainly influenced by the amount of PHBV (higher percentage in the formulations)[25,62]. The observed degradation behaviour of the PHBV/PLA blend was similar to that of the PHBV; this result could be related to the percentage of neat polymers used in this blend (70% PHBV and 30% PLA) (Fig. 7, left). PHBV, PLA, PHBV/PLA and PHBV/PLA/CS/OE/Pgm/ATBC showed single-stage thermal degradation, confirmed by the single peak observed in the DTG curves for these blends (Fig. 7, right). Since the PHBV/PLA blend showed a degradation profile similar to that of neat PHBV (only one peak of degradation), the two-stage degradation profile of the PHBV/PLA/CS blend could be correlated with the degradation of PHBV/PLA and CS. This result was also confirmed by the two peaks observed for this blend in the DTG curves (Fig. 7, right). Even though the 5-component system was a mixture of different components, only one degradation peak was observed

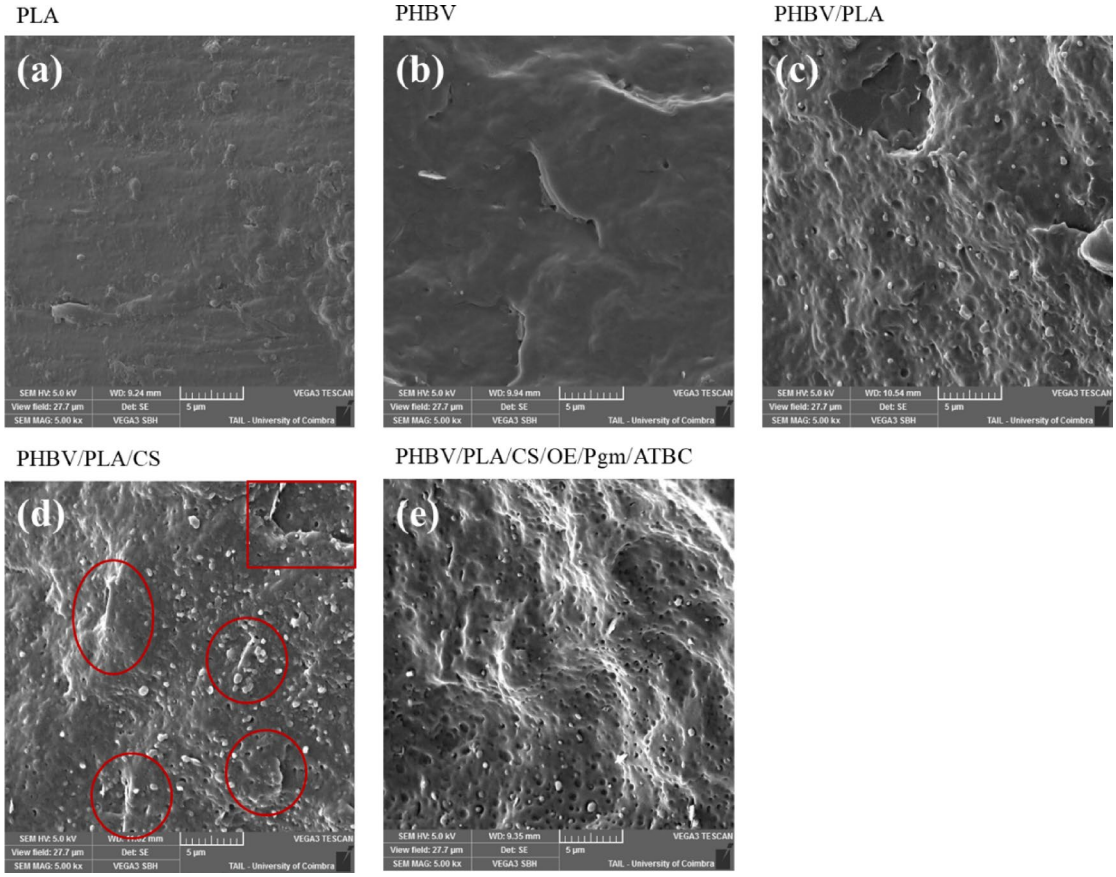

Fig. 6. Scanning electron microscopy (SEM) of the cross-section of neat PLA (**a**), neat PHBV (**b**), formulation of PHBV/PLA (**c**), PHBV/PLA/CS, where is possible to observe the incorporation of CS fibres (red circles) and a place where a CS was pulled off (rectangle) (**d**) and PHBV/PLA/CS/OE/Pgm/ATBC (**e**).

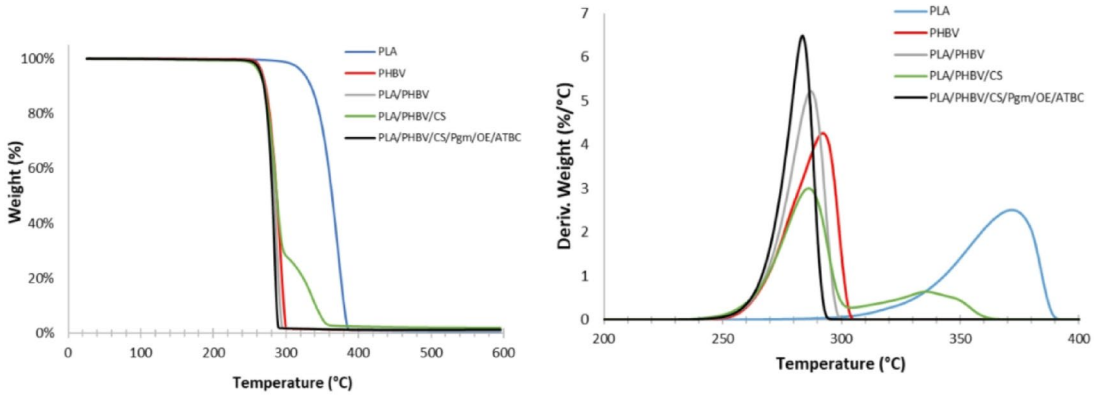

Fig. 7. TGA curves obtained for PLA, PHBV and the developed composites (left) and first derivative (DTG) of TGA curves for the same developed composites.

(Fig. 7, right), and the degradation peak was not observed for CS (as in the PHBV/PLA/CS formulation). CS degradation was reported to start at approximately 220 °C, with a maximum weight loss occurring between 220 and 320 °C[63]; this temperature range falls within the range that we observed in our study. The addition of ATBC to a formulation reduced the thermal stability and shifted the degradation temperature to lower values[64], where the properties of both components (CS and ATBC) influenced the degradation temperature of these two elements. The reported results for the PHBV/PLA/CS/OE/Pgm/ATBC formulation could also be related to the parameters of the analysis, namely, the chosen heating rate. A better resolution of thermal events and understanding of decomposition steps were observed when a slow heating rate was applied; this result was

Formulation	T_2 (°C)	T_p (°C)
PLA	308.6	371.7
PHBV	261.6	292.7
PHBV/PLA	259.6	287.1
PHBV/PLA/CS	254.5	286.2
PHBV/PLA/CS/OE/Pgm/ATBC	258.7	283.6

Table 2. Initial degradation temperature (T_2) and the temperature of the maximum rate of weight loss (T_p) for PLA, PHBV and the developed composites.

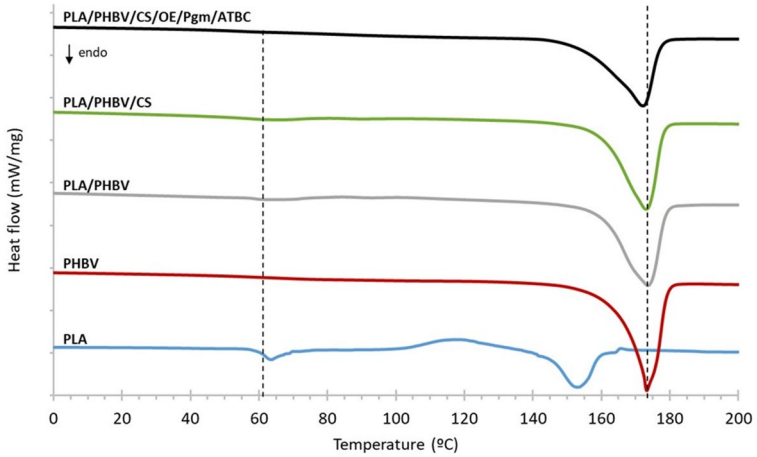

Fig. 8. DSC thermograph curves (2nd heating) of PLA, PHBV and the developed composites.

Formulation	*Tg* (°C)	*Tc* (°C)	Tm (°C)	ΔH_m
PLA	62	118	153	28.8
PHBV	60	-	173	82.3
PHBV/PLA	59	-	174	83.2
PHBV/PLA/CS	58	-	173	75.5
PHBV/PLA/CS/OE/Pgm/ATBC	54	-	172	66.3

Table 3. Thermal transitions detected by DSC for PLA, PHBV and the developed composites.

opposite to the use of a fast heating rate where thermal events could overlap, causing difficulty to observe the different decomposition steps[65]. Considering the complexity of the 5-component formulation, the heating rate selected was likely too high to observe the degradation of each component; here, the parameters of the TGA analysis were the same for all the formulations analysed.

Differential scanning calorimetry (DSC)

Differential scanning analysis is a powerful tool for determining polymer crystallinity, thermal transitions (glass transition, *Tg*; cold crystallization, *Tc*; and melting point, *Tm*) and blend compatibility. For the latter, incompatible blends will show distinct thermal transitions related to each individual phase, whereas compatible blends present a single transition. Figure 8 shows the DSC thermographs of the PLA, PHBV, and PHBV/PLA blends and their compositions, and the corresponding transitions are provided in Table 3. The *Tg* values of neat PLA and PHBV are 62 and 60 °C, respectively, but both have distinct melting peaks (153 and 173 °C). Additionally, PLA has a characteristic cold crystallization peak at approximately 118 °C[66]. When PLA is blended with PHBV, *Tc* disappears, *Tg* is less pronounced, the melting peak is broader on the left side (left shoulder) and the *Tm* value does not change. Both individual melting peaks (in an incompatible blend system) are expected to be observed, but since the *Tm* values of each phase are similar, they overlap, and the calculation of crystallinity is not possible[67]. The addition of CS does not affect the transition temperature but has a negative effect on the melting enthalpy. As expected, the presence of ATBC seems to decrease *Tg* (54 °C) due to its plasticizing effect[49,50]. ATBC molecules can increase the distance between polymer chains, increasing their molecular mobility at lower temperatures[68]. Additionally, an increase in the left should change the melting peak, where the melting peak also shifts to lower values. This is an indication of the higher molecular mobility of the polymeric

Sample	MFR (g/10 min) at 190 °C/2.16 kg
PLA	42.7 ± 2.9
PHBV	13.9 ± 0.7
PHBV/PLA	30.0 ± 1.7
PHVB/PLA/CS	- *
PHVB/PLA/CS/OE/Pgm/ATBC	- *

Table 4. Melt flow rates of the PLA, PHBV, and PHVB/PLA blends and composites at 190 °C with a 2.16 kg weight. *The die was obstructed, and the material did not flow.

Formulation	Tensile strength (MPa)	Yield strain (mm)	Young modulus (MPa)	Strain at break (mm)
PLA	51.9 ± 0.69	0.07 ± 0.00	804.9 ± 3.33	0.07 ± 0.00
PHBV	30.58 ± 0.92	0.04 ± 0.00	823.2 ± 5.79	0.05 ± 0.00
PHBV/PLA	32.17 ± 0.86	0.04 ± 0.00	804.23 ± 10.90	0.05 ± 0.00
PHBV/PLA/CS	25.40 ± 0.91	0.03 ± 0.00	871.23 ± 3.60	0.03 ± 0.00
PHBV/PLA/CS/OE/Pgm/ATBC	19.03 ± 0.92	0.04 ± 0.00	713.96 ± 30.20	0.04 ± 0.00

Table 5. Mechanical properties of PLA, PHBV, and the material composites developed in the different formulations. The results are presented as the average of 5 test specimens (AV ± SE).

phases due to the presence of the plasticizer. While these results suggest that ATBC has a plasticizing effect, further analysis, such as dynamic mechanical analysis (DMA), should be carried out to sustain this hypothesis.

Table 4 lists the MFR values for the examined samples at 190 °C and provided insight into the processing properties of the polymer melt. Neat PLA had a higher MFR (42.7 g/10 min) than PHBV (13.9 g/10 min) and was compatible with an injection polymer grade. Blending PHBV with 30 wt% PLA led to an increase in the MFR, which was expected since PLA is less viscous. However, the MFR of the PHBV/PLA blend remained below that of PLA; these results indicated that the thermomechanical forces from the blending process did not cause significant molecular weight degradation. This behaviour was highly concerning and often observed in thermosensitive polymers, as reported by some authors[69]. Overall, these results supported the deduction that the structural integrity of the polymers was maintained during processing. On the other hand, the incorporation of CS substantially increased the viscosity of the compounds, stopping their flowability through the MFR die. The size of the CS particles played a crucial role in these results. To assess the true influence of all additives on the rheology of blends, further additional rheometry trials need to be performed (such as parallel plates or extensional rheology).

The mechanical properties of the formulations were evaluated at room temperature, and the results are listed in Table 5.

The developed formulation of PHBV/PLA had a tensile strength similar to that of the PHBV alone, but the Young's modulus and the strain at break were more similar to the results obtained for PLA alone. The CS addition increased the Young's modulus of the formulation (PHBV/PLA/CS); these results indicated increased resistance to deformation, and the tensile strength was also reduced. Figure 9 presents the results for tensile strength and Young's modulus of the developed formulations. Before being integrated into the matrix, CS was ground into smaller particles (average size: 0.71 mm ± 0.2; $n = 20$) (Av ± SD); thus, CS had a greater tendency to agglomerate, and weak points where accumulation of stress could occur were formed. The mechanical results for the PHBV/PLA/CS/OE/Pgm/ATBC formulation show a clear reduction in the tensile strength and Young´s modulus of this formulation. This effect should be related to the plasticizing effect of the ATBC that constitutes 10% wt of the formulation (both OE and Pgm are present at a 1% wt in the formulation). With ATBC addition, the intermolecular forces (cohesion) between polymer chains become reduced, while the mobility of polymeric chains increases leading to a decrease in strength and an increase in flexibility and ductility[50,70,71]. During the melt blending, ATBC weakens the bind and entanglement forces between polymer chains by filling the gaps/penetrating between them (decrease in cumulative intermolecular forces), increasing their mobility and therefore the elongation of the composites[50]. The same effect of reduced tensile strength and reduced Young´s modulus of composites when ATBC is added is reported in the literature both for PLA and PHBV composites, while an increase in the elongation at break values are also reported (as in the present study and vs. PHBV/PLA/CS formulation)[50,71,72]. Reported results are common in plasticized systems and usually reinforcements are used to compensate for the loss of strength and modulus[50]. In our study, chitosan fibres were added, leading to an increase in Young´s modulus from 804 MPa to 871 MPa (PHBV/PLA vs. PHBV/PLA/CS) but the tensile strength presents a lower value of 25 MPa (vs. 32 Mpa for PHBV/PLA/CS vs. PHBV/PLA). In the most complex formulation, the ATBC effect was more pronounced than the CS addition, and a decrease in the mechanical properties was observed. The mechanical results found for the developed biocomposites are comparable to those of PP (tensile strength between 31 and 41.4 MPa, Young Modulus between 1140 and 1550 MPa)[73,74] and PE (low-density PE - tensile strength between 8.3 and 31.4 MPa, Young Modulus between 170 and 280 MPa; high-density PE - tensile strength between 22.1 and 31.0 MPa, Young Modulus of 1080 MPa)[74].

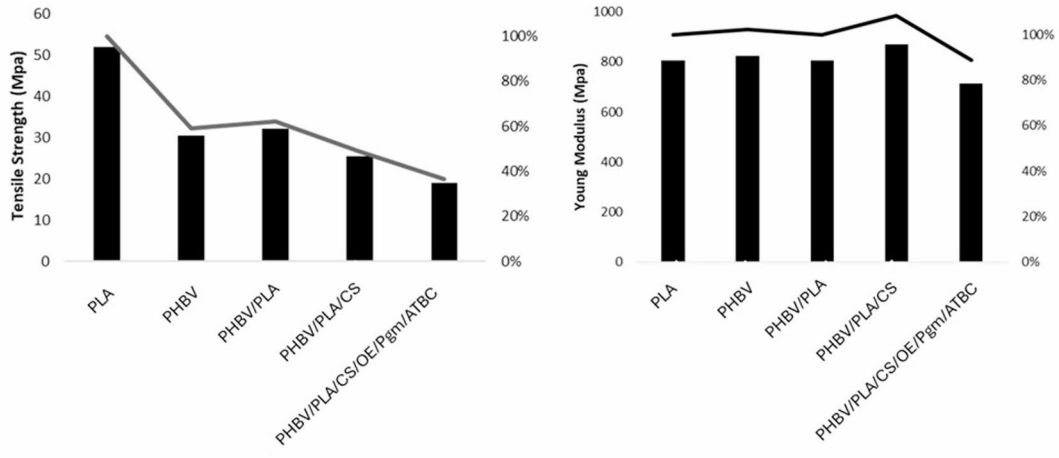

Fig. 9. Mechanical properties of test specimens developed for each formulation: tensile strength (MPa) (left) and the Young Modulus (MPa) (right).

Formulation	Water contact angle (°)
PLA	72.1 ± 1.8
PHBV	77.2 ± 0.5
PHBV/PLA	78.0 ± 2.0
PHBV/PLA/CS	72.4 ± 1.4
PHBV/PLA/CS/OE/Pgm/ATBC	81.5 ± 1.5

Table 6. Water contact angles measured in the test specimens of the different formulations developed.

The hydrophobicity of the developed formulations was assessed using water contact angle measurements. Table 6 provides the measured water contact angles.

Wettability involves the measurement of contact angles between the sample and the water drop (degree of wetting when a solid and a liquid interact); additionally, a large contact angle (≥ 90°) is indicative of low wettability (hydrophobicity, fluid minimizes contact with the surface), and a small contact angle (≤ 90°) is indicative of high wettability (hydrophilicity, fluid spreads over a large area of the surface)[75]. After the analysis was performed with water, all samples exhibited hydrophilic behaviour since all the samples had contact angles of less than 90°[75]. The measured water contact angles for the different test specimens tested for each formulation did not show a high variation. PLA had a water contact angle of 72.1° (Fig. 10a)). The reported value for this polymer was in agreement with that reported in the literature, which usually ranges between 60 and 85° (for the same material)[76–78]. Several factors could account for changes in contact angle values and include surface impurities, chemical surface composition, roughness, and wetting of the test specimens (the wettability of PLA depends mostly on the surface roughness)[76]. The SEM results revealed a flat surface for the PLA test specimen at the fracture location (Fig. 6. a)). PLA wettability also depended on its crystallinity, and high-crystallinity polymers show higher water contact angles[77]. Usually, the lower crystallinity of polymers (amorphous regions) results in more hydrophilic surfaces due to higher surface energy and increased surface polarity, leading to lower water contact angles[79]. The PLA used in our study was reported to be amorphous, with no crystallization (high level of homogeneity) (Fig. 3); this was in agreement with our results. For PHBV (Fig. 10. b)), which had a relatively high level of crystallinity, the measured water contact angle (77.2° ± 0.5°) was in agreement with that reported in the literature for the same material (washed with deionized water): Meereboer et al.[80]. reported a water contact angle of 66.7°, and Snowdon et al.[78]. reported a water contact angle of 67.46° ± 0.29°. For the PHBV/PLA and the PHBV/PLA/CS formulations, the measured water contact angles were 78.0° ± 2.0° and 72.4° ± 1.4°, respectively. The contact angle found for PHBV/PLA was closer to the PHBV than the water contact angle measured for PLA; this result was reasonable if the formulation, which consisted of 70% PHBV and 30% PLA was considered (Fig. 10c)). The X-ray scattering data (Fig. 5) indicate that the crystal structure of PHBV was similar to that of the neat PHBV alone and that PLA (no crystallization) was incorporated into the amorphous phase of PHBV. The previous results could aid in explaining these results. The integration of CS in the formulations (PHBV/PLA/CS) (Fig. 10.d)) slightly decreased the water contact angle (vs. PHBV/PLA), indicating the hydrophilic nature of this component[81]. The 5-component system presented a higher measured value for the water contact angle (Fig. 10e). X-ray scattering results indicated the integration of PLA in the amorphous region of the PHBV (with a similar crystal structure to that of the PHBV alone and to the previously described formulation). For the pigment (phycocyanin-soluble) and the plant oil (hydrophobic), 1% of each was used in the 5-component formulation; these components had little to no effect on the water contact angle measured because part of the

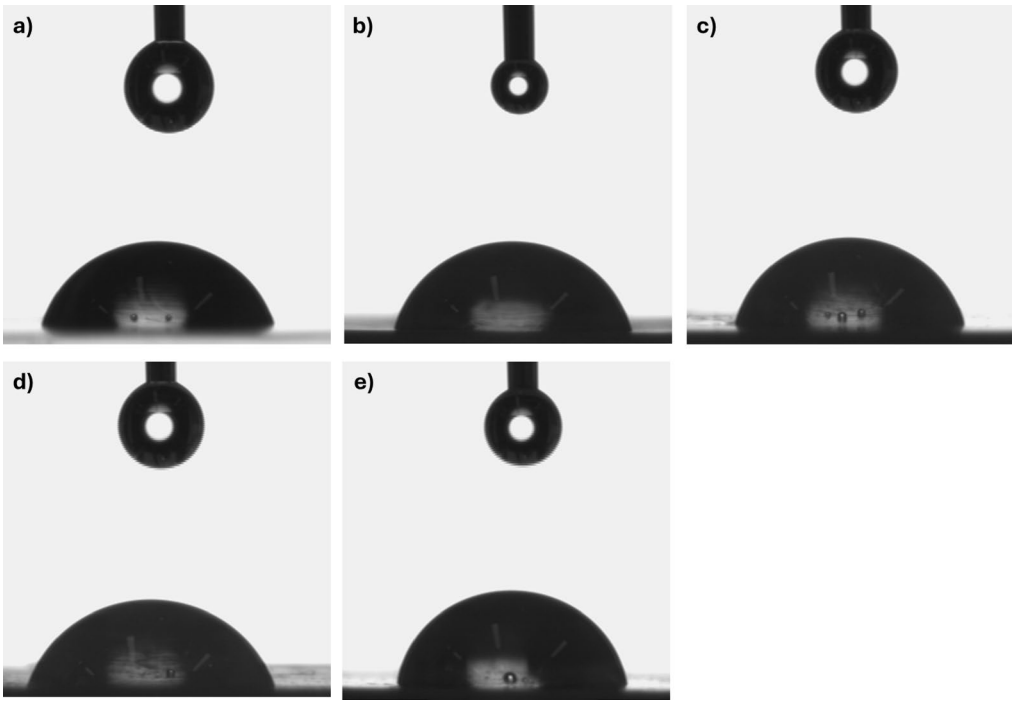

Fig. 10. Measured water contact angle for the different developed formulations: (**a**) PLA; (**b**) PHBV; (**c**) PHBV/PLA; (**d**) PHBV/PLA/CS; (**e**) PHBV/PLA/CS/OE/Pgm/ATBC.

plant oil could be degraded during the injection process. ATBC, which is hydrophobic[82], constituted 10% of the formulation. The X-ray scattering results indicated the integration of ATBC in the amorphous phase of PHBV (shown also by the larger presence in the scattering curves of the PHBV/PLA/CS/OE/Pgm/ATBC). The changes in the WCA could be attributed to the addition of ATBC, which was the major difference from the other formulations. Another important factor described briefly previously was the roughness of the test specimen surface. Higher roughness is related to increasing WCA values by reinforcing the hydrophobic nature of the surface[76]. As observed in the SEM images (Fig. 6e), the 5-component formulation had a surface with the most irregularities and roughness.

Due to their hydrophilic nature, the developed materials could be more prone to hydrolytic degradation, providing a potential advantage.

Figure S7 (and video content) shows the first printing of an object base, cosmetic packaging in a new composite material. Cosmetic packaging production is usually associated with techniques such as injection moulding, and blow moulding, among others, but 3D printing is the future and presents several advantages. 3D printing allows for the personalization and customization of products, in a rapid prototyping scenario which reduces the costs and reliance on traditional tooling and prototyping methods leading to a shorter product development cycle and shorter time to market. This was the first test experiment that needed the optimized parameters and compounds; traditional injection processes (which have already been widely validated) also need to use optimized parameters. Notably, although we are dealing with digital and current technologies, the development and optimization of both materials and optimal processing parameters are crucial. Current work is in progress to ensure that the adjustment among the parameters, materials, and objects will occur. One of the major difficulties encountered was the processing temperature, where an equilibrium needs to be reached to process all constituents in the formulation without losing properties or leading to the degradation of the material. Initially, a temperature of 185 °C was used, but extrusion of the material was not possible at this temperature; thus, the temperature was increased by 5 degrees at a time until reaching 200 °C. At this temperature, the materials still could not be printed. The temperature was increased again but at a lower rate: one degree at a time until 206 °C, where the material had degraded. The optimal working temperature for printing the base for cosmetic packaging was determined to be 205 °C (Figure S7). During the printing process, ATBC was added to the mixture of pellets to facilitate the process, but careful considerations were needed due to heat dissipation, ATBC could also impair the process; the pellets would not flow naturally to the equipment because due to heat dissipation in the feeding hoppers, cohesion between pellets occurred where ATBC was added. The printing process for the developed material still needs optimization. Figure S7 shows the difference in colour between the pellets and the base for the cosmetic packaging. The differences observed were likely related to the degradation of the constituents, namely, the natural pigments used. A similar colour change was observed for the test specimens obtained during the injection process. Colour measurement was performed to understand colour differences in pellet samples (PHBV/PLA/CS/OE/Pgm/ATBC) before processing (injection moulding or 3D printing), injection moulded test specimens' samples (PHBV/PLA, PHBV/PLA, CS and PHBV/PLA/CS/OE/Pgm/ATBC) and 3D printed base sample. The CIELAB (L*, a*, b*) colour results for the different samples tested are present in Table 7.

Formulation	Type of sample	L*	a*	b*
PHBV/PLA	Test specimen	89	0	15
PHBV/PLA/CS	Test specimen	83	3	14
PHBV/PLA/CS/OE/Pgm/ATBC	Test specimen	70	1	11
	Pellets	70	−5	−13
	3D printed base	78	−3	8

Table 7. CIELAB colour measurement results for different samples tested.

Formulation/label	PHBV (wt %)	PLA (wt %)	Chitosan (wt %)	Pigment (wt %)	Essential oil (wt %)	ATBC (wt %)
PLA	0	100	0	0	0	0
PHBV	100	0	0	0	0	0
PHBV/PLA	70	30	0	0	0	0
PHBV/PLA/CS	70	25	5	0	0	0
PHBV/PLA/CS/OE/Pgm/ATBC	65	18	5	1	1	10

Table 8. Different polymer blends developed and the weight ratios of their constituents.

The colour measurement results indicate a difference in colour between the different tested samples. After the addition of essential oil (OE), natural pigment (Pgm) and ATBC, the materials (PHBV/PLA/CS/OE/Pgm/ATBC) present a darker colour (vs. PHBV/PLA & PHBV/PLA/CS test specimens' samples), with the test specimen and the pellet samples presenting the same values for lightness.

Materials and methods

Materials

PHBV, under the trade name Enmat Y1000, supplied by Helian Polymers (Belfeld, The Netherlands) in pellet form, was used. It is a 100% biodegradable polymer with the following characteristics (as supplied by the company): melting point of 175–180 °C, elongation at break of 3.8%, tensile strength of 39 MPa, and density of 1.25 g/cm^3. The PLA (in pellets) was provided by NatureWorks (Minnetonka, USA) with the trade name Ingeo™ Biopolymer 3052D and has the following properties: a crystalline melting temperature between 145 and 160 °C, a tensile elongation of 3.5%, a tensile yield strength of 62 MPa and a density of 1.25 g/cm^3. The CS used in the development of the present material composite was provided by the company Kitosano (Bajo Guadalquivir district in Andalusia, Spain), with a degree of deacetylation of 86%. CS had a white pale/translucid colour before any processing. The plant oils used in the development of this formulation were acquired from Herdade de Vale do Côvo with the certification ECOCERT (PT-BIO-02) for ingredients of natural origin. The natural pigment used was phycocyanin, a blue spirulina purchased from Bluetec Naturals. The citrate used was ATBC from Wuxi Philchem New Materials Co., Ltd. (CAS: 77-90-7).

Composite Preparation and processing techniques

Materials pretreatment

For the results reported in this study, PHBV and PLA were used as the matrix. Pellets from PHBV and PLA, which are both biodegradable polymers, were dried in an oven at 60 °C for at least 12 h before use to ensure that they were dry. CS was ground to make smaller fibres with the help of a grinder (average size of 0.71 mm ± 0.2; $n = 20$) (Av ± SD), so they could be more easily incorporated into the material composite, and to promote the homogeneity of the mixture. The different formulations were prepared in different ratios and selected based on the literature and acquired knowledge (Table 8).

Extrusion processing techniques

The formulations PHBV/PLA, PHBV/PLA/CS and PHBV/PLA/CS/Pgm/ATBC were mixed at the appropriate ratios using a corotating twin extruder (Werner & PfleidererZSK25 × 38D) with a screw diameter of 25 mm and a maximum rotation of 300 rpm. The equipment is constituted of rollers, a water tank to cool the material and a granulator which enables cutting the developed filament coming out of the die into granules. The equipment has a screen pack (mesh), and a nitrogen purge is present in the feeder and the material was extruded using a range of temperatures per zone between 150 and 180 °C. For the PHBV/PLA/CS formulation, after CS was ground, it was added to the appropriate amounts of PHBV and PLA. The PHBV/PLA/CS/OE/Pgm/ATBC mixture was prepared as follows: the PHBV, PLA and CS were added together in a container and homogenized (by hand), the pigment (phycocyanin) was added, and the mixture was homogenized again. In a separate glass beaker, the essential oil and ATBC were added together and mixed. Then, this solution containing essential oil and ATBC was added to the previous mixture (of PHBV, PLA, CS and pigment), and a final mixture/homogenization of the formulation was performed. The mixtures were compounded by using a corotating twin-screw extruder (same as previously used). The extruded filamentary composites were subsequently cut into pellets for use in the injection machine.

Injection parameters	PHBV	PLA	PHBV/PLA	PHBV/PLA/CS	PHBV/PLA/CS/OE/Pgm/ATBC
Temperature range (°C)	200 – 170	180 – 160	200 – 170	220 – 170	200 – 170
Cycle time (s)	65	115	65	65	65
Speed (cm^3/s)	30	38	36	30	25
Size shot (cm^3)	4.5	7.5	5	5	5
1 st Pressure (Bar)	550	1100	500	600	500
Back Pressure (bar)	788	788	788	788	788

Table 9. Formulations performed and parameters that were used for the injection process of each formulation.

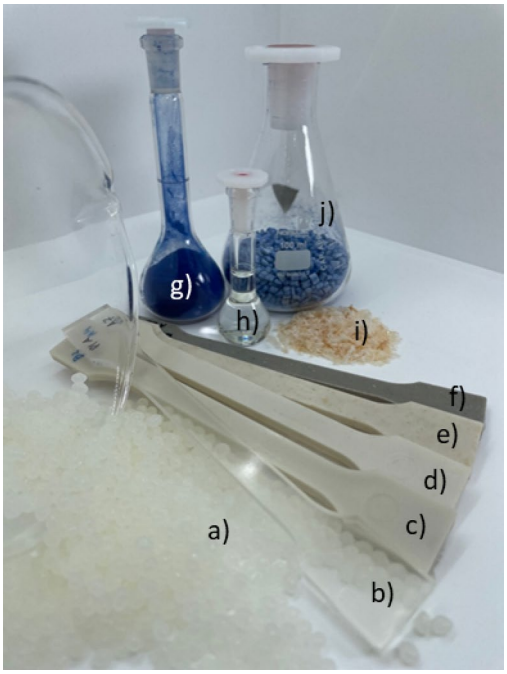

Fig. 11. Biomaterials used in the formulation of the selected composites. (**a**) PLA pellets; (**b**) PLA test specimen; (**c**) PHBV test specimen; (**d**) PHBV/PLA test specimen; (**e**) PHBV/PLA/CS test specimen; (**f**) PHBV/PLA/CS/phycocyanin (Pgm)/ATBC/plant essential oil (OE) test specimen); (**g**) phycocyanin; (**h**) ATBC/plant Solution; (**i**) chitosan; (**j**) PHBV/PLA/CS/phycocyanin (Pgm)/plant essential oil pellets.

Injection moulding processing techniques

The composite dumbbell-shaped standard test specimens (ISO 527-2:2012)[83] were prepared by an injection moulding machine (BOY 22 A, Germany) projected for the processing of thermoplastics and elastomers, among other materials. The processing parameters for the injection were initially selected based on the technical data sheets for each polymer used, and then an optimization step was performed due to adjustments to the formulations. The dimensions of the test specimens prepared were width at narrow section – 10 mm; width at the ends- 20 mm; thickness- 4 mm; overall length- 150 mm; gauge length 50 mm. The test specimens obtained in this work were greyish and did not have a strong smell. The parameters used for the injection of the test specimens of each formulation are listed in Table 9. Figure 11 shows the biomaterials used for the development of the described composites.

Additive manufacturing technology

Additive manufacturing technologies have been used widely in different industries, where this technology has several advantages over more traditional technologies. Additive manufacturing allows for the creation of complex geometries of physical objects directly from digital concepts, with good material efficiency and low consumption costs[84]. Moreover, material use is optimized, and waste is reduced. AM technologies have been continuously evolving because in addition to the reported benefits, this technology contributes to different aspects of sustainability and allows for the integration of circularity principles[84]. Stratasys developed and patented fused deposition modelling (FDM) 3D printing technology in 1989[85]. This technology was based on the controlled extrusion of thermoplastics using a solid thermoplastic filament that was sequentially melted and deposited to make the shape of the object. In 2009, the Stratasys patent expired, and thermoplastic deposition systems were developed everywhere due to the development of freeware software such as cura, slic3r, simplify, kisslicer and others. Thermoplastic extrusion occurred with the melting of the pellets. This technology has been used for half a

dozen years. Specifically, extrusion is not based on filaments (filaments are made by extrusion pellets) but rather on pellets and screw extruders. This ability to directly produce parts and objects from pellets allows for a greater diversity of available materials, as well as the dimensions of the components to be produced. Today, extruders are based on screws in 3D printing machines that process 500 kg/hour. The technological novelty of using an older technology is suited to today's machines and methods; however, improvements are still needed. This path provides the possibility of more easily exploring the limits of the development of thermoplastic matrix materials and composites, and at the same time, this path has a major challenge. The described technology enables the large-scale production of different products with the benefit of testing different designs. In addition, one of our goals was to examine the developed material in a prototype. For that purpose, the material composites developed in this work were tested for additive manufacturing of cosmetic packaging using a 3D printer (Piocreat G5 FGF) with fused granular fabrication (FGF) technology. The initial temperature was set to 185 °C, and the material was printed at a speed of 20 mm/s through an adapted nozzle of 1.8 mm.

Material characterization techniques

Infrared absorption spectroscopy

The vibrational analysis of the samples was carried out using Fourier transform infrared (FTIR) spectroscopy via reflectance, using the non-destructive sampling technique of attenuated total reflectance (ATR). The infrared spectra (4000–550 cm^{-1}) of the samples at room temperature were recorded using a Perkin Elmer Frontier spectrometer (FT-NIR/MIR) equipped with an FR-DTGS detector and a KBr beam splitter. The spectra were recorded at a resolution of 4.0 cm^{-1} with 128 accumulations (scans). A Perkin Elmer sampling accessory with a universal attenuated total reflectance (UATR) module with a diamond/ZnSe crystal was used, and a constant force of 110 N was applied to all the recordings. The samples were analysed without any treatment.

X-ray scattering

Wide-angle X-ray scattering (WAXS) and small-angle X-ray scattering (SAXS) measurements of the structure and morphology of the injection moulded test specimens were performed on the NCD-SWEET beamline at the ALBA Synchrotron Light Source in Barcelona, Spain[86,87]. The X-ray source in an in-vacuum undulator driven by the 3GeV storage ring produces numerous harmonics. In this work, we exploited the 7th harmonic with an energy of 12.4 keV and a wavelength of 1 Å. A transmission geometry was employed with the long axis of the moulded part mounted vertically. The SAXS intensity patterns were recorded with a Pilatus 1 M system from DECTRIS. This detector has an effective pixel size of 172 × 172 micrometres with a dynamic range of 20 bits. The sample-to-SAXS detector distance was 6.6659 m from the sample. The flight path from the sample to the detector was a low vacuum vessel, which eliminated the majority of the air from the flight path. The WAXS detector (a Rayonic LX255HS CCD system) was mounted above the X-ray beam path and tilted towards the sample. As a consequence, data with scattering vector magnitudes of 0.29 to 7.96 Å could be measured. The WAXS detector distance, tilt angle and pixel size were calibrated using Cr_2O_3. The modulus of the scattering vector Q is given by $Q = 4\pi\sin\theta/\lambda$, where 2θ is the scattering angle and λ is the incident beam wavelength. The SAXS patterns were measured over a $|Q|$ range from 0.017 $Å^{-1}$ to 0.125 $Å^{-1}$. The detector pixel size and sample-to-detect ratio were calibrated with the well-known standard AgBh[8]. For both SAXS and WAXS, 2D data were collected and were easily converted for isotropic data to a radial average as a function of the modulus of the scattering vector Q.

For the polyhydroxybutyrate sample, we also conducted operando X-ray scattering measurements during an injection moulding cycle using equipment recently developed at CDRSP. Data collection was restricted to the SAXS detector. The apparatus enabled data to be accumulated at 1 s intervals during the completed injection moulding cycle. The apparatus was essentially what has already been described in the literature. The mould cavity was designed to produce a part that was 1 mm thick, 70 mm long and 20 mm wide. The mould cavity was fabricated from an aluminium/manganese alloy. A standard industry recirculating water unit was used to maintain the mould temperature of 65 °C. A Babyplast injection unit from Rambaldi was used to perform the injection with the following parameters: shot size, 4.5 cm^3; 1 st pressure, 150 bar for 25 s; and 2nd pressure, 150 bar for 6 s.

The moulded sample was mounted on a translation stage, which enabled measurements at three equidistant points along the centre line of the long axis of the sample. The small-angle X-ray scattering data were recorded simultaneously with the wide-angle X-ray scattering data. The primary data were displayed as a false colour image of the intensity recorded on the pixelated detector. The long axis of the detector corresponded to the scattering angle of 2θ, whereas the azimuthal variation corresponded to the arc bands of intensity.

Scanning electron microscopy (SEM)

Sections of the test specimens were analysed using scanning electron microscopy (SEM; TESCAN VEGA 3 SBH - Easy Probe SEM with a tungsten-heated cathode). SEM images were acquired with a working voltage of 5 kV and a secondary electron detector. Since our samples were not conductive, they were sputter coated with a 10 nm thick gold/palladium layer using the Quorum SC7620- Mini Sputter Coater/Glow Discharge System prior to SEM analysis. The cross-sections of the composite material were observed.

Thermogravimetric analysis (TGA)

A thermal analysis (TA) instrument (model Q500) was used to perform thermogravimetric analysis of the different specimens to understand their thermal stability. Small samples from the extruded material (pellets) of the different formulations developed were chosen and used in the analysis. For this purpose, a small pellet of each formulation was placed inside a crucible and heated from 25 °C to 600 °C at a heating rate of 10 °C/min. An inert atmosphere was maintained by providing a flow of nitrogen gas at a rate of 60 ml/minute. The maximum degradation percentage and weight loss were obtained by graphical means.

Differential scanning calorimetry (DSC)
Differential scanning calorimetry (DSC) was performed using a TA instruments (DSC 250 Discovery Series with computer software for analysis TA Instruments, Trios) to examine the melting and crystallization temperatures of the crystalline phase. The examination occurred at temperatures ranging between − 20 °C and 250 °C under a nitrogen atmosphere (100 ml/minute). All measurements were performed according to the following program: equilibration at −20 °C followed by heating at a rate of 10 °C/minute until 250 °C was reached. A first heating cycle was performed to erase the thermal history of the samples; however, for the results, we considered only the second heating cycle. The glass transition temperature was determined using the inflection-point method, as described in the ISO 11357-2 standard[88].

Melt flow rate (MFR)
The MFR analysis of the specimens was performed by using a Daventest Serial N°3/2606 equipment according to the ISO 1133-1:2022 standard[89]. The characterization was performed at 190 °C using a 2.16 kg weight.

Mechanical properties testing
The tensile strengths of the specimens were measured according to the ISO 527- 2:2012 standard[83] using a tensile machine (INSTRON 4505) (with a 5 kN load cell) that was equipped with a wedge-action tensile clamp. The tensile test was performed at room temperature on 5 test specimens of each formulation, and the results were averaged. A speed of 1 mm/minute was used to perform the tensile tests.

Water contact angle (WCA)
WCA was recorded with an OCA-20 tensiometer (Dataphysics, Germany) and extracted with SCA20 software. Here, 10 µL drops were dispersed on each injected test specimen, with at least 6 replicates per treatment. The data were obtained at room temperature by the sessile method, and the contact angle was measured 2–3 s after drop deposition. The test specimens were rinsed with distilled water and dried with a paper towel before analysis.

Colour measurement
A colour measurement was carried out using an NCS (NaturalColor System) digital colour reader (NCS colourpin II, Sweden) connected to a database via a smartphone application. Colour changes measurements were performed using samples of pellets (PHBV/PLA/CS/OE/Pgm/ATBC formulation), samples of test specimens (all blends), and a sample of the 3D printed base to assess colour changes related to the constituents and to the processing method (injection moulding and 3D printing). The natural colours system results were converted to the CIELAB standard using the information provided by the application.

Conclusions
Material composites composed of biobased polymers and natural constituents were developed and characterized in terms of their structure, topography, thermal stability, mechanical properties, and hydrophobicity. PLA is an amorphous material, and PHBV is semicrystalline; notably, in the developed mixtures (PHBV/PLA/CS and PHBV/PLA/CS/OE/Pgm/ATBC), PLA and ATBC were not crystallized and were integrated into the amorphous phase of the PHBV polymer. The thermal analysis indicated that PLA had the highest thermal stability, but for PHBV and the other developed material composites, the thermal degradation began at approximately the same temperature. In the results obtained for the PHBV/PLA/CS formulation, two degradation peaks were observed and corresponded to the polymers and CS degradation. The same result was not observed for the 5-component system. The addition of CS did not affect the transition temperatures, and the addition of ATBC decreased the *Tg* by increasing the mobility of the polymer chains at lower temperatures. In terms of mechanical properties, the CS addition reduced the tensile strength but increased the resistance to deformation. The addition of other additives to the formulation, mainly ATBC (OE and Pgm constituted 1% wt each) slightly increased the yield strain but showed a reduction in tensile strength and in the young modulus. All developed composites were hydrophilic and more prone to hydrolytic degradation, and the 5-component system was the least hydrophilic material developed. Based on our results, biobased material composites were developed with the addition of inexpensive and available industry-by-product (CS); these materials have an attractive natural colour and smell with possible applications in cosmetic industry packaging (as a substitute for fossil-based materials) and could be produced from additive manufacturing technologies, although this technology still presents a lot of investigation to be done, it shows promising results.

Data availability
All data generated or analysed during this study are included in this published article (and its Supplementary Information files).

Received: 22 January 2025; Accepted: 3 July 2025
Published online: 24 July 2025

References
1. Gatt, I. J. & Refalo, P. 'Reusability and recyclability of plastic cosmetic packaging: A life cycle assessment', *Resources, Conservation & Recycling Advances*, vol. 15, p. 200098, Nov. (2022). https://doi.org/10.1016/j.rcradv.2022.200098
2. Atiwesh, G., Mikhael, A., Parrish, C. C., Banoub, J. & Le, T. A. T. 'Environmental impact of bioplastic use: A review', *Heliyon*, vol. 7, no. 9, p. e07918, Sep. (2021). https://doi.org/10.1016/j.heliyon.2021.e07918
3. E. a sustainable future Plastics Europe, 'Plastics – the fast Facts 2024', *2024 Plastics Europe AISBL*, [Online]. (2024). Available: https://plasticseurope.org/wp-content/uploads/2024/11/PE_TheFacts_24_digital-1pager.pdf

4. Reichert, C. L. et al. Jul., 'Bio-Based Packaging: Materials, Modifications, Industrial Applications and Sustainability', *Polymers*, vol. 12, no. 7, p. 1558, (2020). https://doi.org/10.3390/polym12071558
5. Curia, S. et al. Oct., 'Betulin-Based Thermoplastics and Thermosets through Sustainable and Industrially Viable Approaches: New Insights for the Valorization of an Underutilized Resource', *ACS Sustainable Chem. Eng.*, vol. 7, no. 19, pp. 16371–16381, (2019). https://doi.org/10.1021/acssuschemeng.9b03471
6. Arijeniwa, V. F. et al. Closing the loop: A framework for tackling single-use plastic waste in the food and beverage industry through circular economy- a review. *J. Environ. Manage.* **359**, 120816. https://doi.org/10.1016/j.jenvman.2024.120816 (May 2024).
7. Mazur, K. E., Jakubowska, P., Gaweł, A. & Kuciel, S. Mechanical, thermal and hydrodegradation behavior of Poly (3-hydroxybutyrate-co-3-hydroxyvalerate) (PHBV) composites with agricultural fibers as reinforcing fillers. *Sustainable Mater. Technol.* **31**, e00390. https://doi.org/10.1016/j.susmat.2022.e00390 (Apr. 2022).
8. Guillot, J. D. 'Plastic waste and recycling in the EU: facts and figures', *Directorate General for Communication - European Parliament*, no. 20181212STO21610, p. 6, Jun. 25, 2024.
9. Greenpeace *Circular Claims Fall Flat again- 2022 Update* (Greenpeace, Oct. 2022).
10. Stark, N. M. & Matuana, L. M. Trends in sustainable biobased packaging materials: a mini review. *Mater. Today Sustain.* **15**, 100084. https://doi.org/10.1016/j.mtsust.2021.100084 (Nov. 2021).
11. Nouri, A., Wang, L., Li, Y. & Wen, C. Materials and manufacturing for Ankle–Foot orthoses: A review. *Adv. Eng. Mater.* **25** (20), 2300238. https://doi.org/10.1002/adem.202300238 (Oct. 2023).
12. Patel, M. K. et al. Nov., 'Improvement of Poly(lactic acid)-Poly(hydroxy butyrate) Blend Properties for Use in Food Packaging: Processing, Structure Relationships', *Polymers*, vol. 14, no. 23, p. 5104, (2022). https://doi.org/10.3390/polym14235104
13. Siracusa, V. & Blanco, I. 'Bio-Polyethylene (Bio-PE), Bio-Polypropylene (Bio-PP) and Bio-Poly(ethylene terephthalate) (Bio-PET): Recent Developments in Bio-Based Polymers Analogous to Petroleum-Derived Ones for Packaging and Engineering Applications', *Polymers*, vol. 12, no. 8, p. 1641, Jul. (2020). https://doi.org/10.3390/polym12081641
14. Morel, S., Mura, G., Gallarate, M. & Sapino, S. 'Cosmetic Packaging: European Regulatory Aspects and Sustainability', *Cosmetics*, vol. 11, no. 4, p. 110, Jun. (2024). https://doi.org/10.3390/cosmetics11040110
15. Vassallo, N. & Refalo, P. 'Reducing the Environmental Impacts of Plastic Cosmetic Packaging: A Multi-Attribute Life Cycle Assessment', *Cosmetics*, vol. 11, no. 2, p. 34, Feb. (2024). https://doi.org/10.3390/cosmetics11020034
16. Porta, R., Sabbah, M. & Di Pierro, P. 'Bio-Based Materials for Packaging', *IJMS*, vol. 23, no. 7, p. 3611, Mar. (2022). https://doi.org/10.3390/ijms23073611
17. Jiang, L., Wolcott, M. P. & Zhang, J. 'Study of Biodegradable Polylactide/Poly(butylene adipate-co-terephthalate) Blends', *Biomacromolecules*, vol. 7, no. 1, pp. 199–207, Jan. (2006). https://doi.org/10.1021/bm050581q
18. Ishimwe, S. & 'BIOPLASTICS MARKET DEVELOPMENT UPDATE. European Bioplastics e.V. Accessed: Mar. 04, 2024. [Online]. (2023). Available: https://www.european-bioplastics.org/bioplastics-market-development-update-2023-2/
19. Abrha, H. et al. Apr., 'Bio-Based Plastics Production, Impact and End of Life: A Literature Review and Content Analysis', *Sustainability*, vol. 14, no. 8, p. 4855, (2022). https://doi.org/10.3390/su14084855
20. Sharma, S. 'Polylactic acid (PLA) and its composites: an Eco-friendly solution for packaging', in Sustainable Food Packaging Technology, 1st ed., Wiley, 107–132. doi: https://doi.org/10.1002/9783527820078.ch4. (2021).
21. Malek, N. S. A. et al. Preparation and characterization of biodegradable polylactic acid (PLA) film for food packaging application: A review. *J. Phys. : Conf. Ser.* **1892** (1), 012037. https://doi.org/10.1088/1742-6596/1892/1/012037 (Apr. 2021).
22. Joseph, T. M. et al. 3D printing of polylactic acid: recent advances and opportunities. *Int. J. Adv. Manuf. Technol.* **125**, 3–4. https://doi.org/10.1007/s00170-022-10795-y (Mar. 2023).
23. Adli, S. A. et al. Jul., 'Development of Biodegradable Cosmetic Patch Using a Polylactic Acid/Phycocyanin–Alginate Composite', *Polymers*, vol. 12, no. 8, p. 1669, (2020). https://doi.org/10.3390/polym12081669
24. Krobot, Š. et al. May., 'Poly(3-hydroxybutyrate) (PHB) and Polycaprolactone (PCL) Based Blends for Tissue Engineering and Bone Medical Applications Processed by FDM 3D Printing', *Polymers*, vol. 15, no. 10, p. 2404, (2023). https://doi.org/10.3390/polym15102404
25. Zembouai, I. et al. Poly(3-Hydroxybutyrate-co-3-Hydroxyvalerate)/Polylactide blends: thermal stability, flammability and Thermo-Mechanical behavior. *J. Polym. Environ.* **22** (1), 131–139. https://doi.org/10.1007/s10924-013-0626-7 (Mar. 2014).
26. Zhao, H., Cui, Z., Sun, X., Turng, L. S. & Peng, X. 'Morphology and Properties of Injection Molded Solid and Microcellular Polylactic Acid/Polyhydroxybutyrate-Valerate (PLA/PHBV) Blends', *Ind. Eng. Chem. Res.*, vol. 52, no. 7, pp. 2569–2581, Feb. (2013). https://doi.org/10.1021/ie301573y
27. Rajan, K. P., Thomas, S. P., Gopanna, A. & Chavali, M. 'Polyhydroxybutyrate (PHB): A standout biopolymer for environmental sustainability', in Handbook of Ecomaterials, (eds Martínez, L. M. T., Kharissova, O. V. & Kharisov, B. I.) Cham: Springer International Publishing, 1–23. doi: https://doi.org/10.1007/978-3-319-48281-1_92-1. (2018).
28. Bharti, S. & Swetha, G. Need for bioplastics and role of biopolymer PHB: A short review. *J. Pet. Environ. Biotechnol.* **07** (02). https://doi.org/10.4172/2157-7463.1000272 (2016).
29. McAdam, B., Brennan Fournet, M., McDonald, P. & Mojicevic, M. 'Production of Polyhydroxybutyrate (PHB) and Factors Impacting Its Chemical and Mechanical Characteristics', *Polymers*, vol. 12, no. 12, p. 2908, Dec. (2020). https://doi.org/10.3390/polym12122908
30. Dwivedi, R., Pandey, R., Kumar, S. & Mehrotra, D. Poly hydroxyalkanoates (PHA): role in bone scaffolds. *J. Oral Biology Craniofac. Res.* **10** (1), 389–392. https://doi.org/10.1016/j.jobcr.2019.10.004 (Jan. 2020).
31. Saha, T., Hoque, M. E. & Mahbub, T. 'Biopolymers for sustainable packaging in food, cosmetics, and pharmaceuticals', in Advanced Processing, Properties, and Applications of Starch and Other Bio-Based Polymers, Elsevier, 197–214. doi: https://doi.org/10.1016/B978-0-12-819661-8.00013-5. (2020).
32. Kulka, K. & Sionkowska, A. 'Chitosan Based Materials in Cosmetic Applications: A Review', *Molecules*, vol. 28, no. 4, p. 1817, Feb. (2023). https://doi.org/10.3390/molecules28041817
33. Bakshi, P. S., Selvakumar, D., Kadirvelu, K. & Kumar, N. S. Chitosan as an environment friendly biomaterial – a review on recent modifications and applications. *Int. J. Biol. Macromol.* **150**, 1072–1083. https://doi.org/10.1016/j.ijbiomac.2019.10.113 (May 2020).
34. Silva, A. O., Cunha, R. S., Hotza, D. & Machado, R. A. F. 'Chitosan as a matrix of nanocomposites: A review on nanostructures, processes, properties, and applications', *Carbohydrate Polymers*, vol. 272, p. 118472, Nov. (2021). https://doi.org/10.1016/j.carbpol.2021.118472
35. Zhang, S. et al. Application status and technical analysis of chitosan-based medical dressings: a review. *RSC Adv.* **10** (56), 34308–34322. https://doi.org/10.1039/D0RA05692H (2020).
36. Abd El-Hack, M. E. et al. Antimicrobial and antioxidant properties of Chitosan and its derivatives and their applications: A review. *Int. J. Biol. Macromol.* **164**, 2726–2744. https://doi.org/10.1016/j.ijbiomac.2020.08.153 (Dec. 2020).
37. Fakhri, E. et al. Nov., 'Chitosan biomaterials application in dentistry', *International Journal of Biological Macromolecules*, vol. 162, pp. 956–974, (2020). https://doi.org/10.1016/j.ijbiomac.2020.06.211
38. Casadidio, C. et al. Chitin and chitosans: characteristics, Eco-Friendly processes, and applications in cosmetic science. *Mar. Drugs.* **17** (6), 369. https://doi.org/10.3390/md17060369 (Jun. 2019).
39. Piekarska, K., Sikora, M., Owczarek, M., Jóźwik-Pruska, J. & Wiśniewska-Wrona, M. 'Chitin and Chitosan as Polymers of the Future—Obtaining, Modification, Life Cycle Assessment and Main Directions of Application', *Polymers*, vol. 15, no. 4, p. 793, Feb. (2023). https://doi.org/10.3390/polym15040793

40. Turek, C. & Stintzing, F. C. 'Stability of Essential Oils: A Review', *Comprehensive Reviews in Food Science and Food Safety*, vol. 12, no. 1, pp. 40–53, Jan. (2013). https://doi.org/10.1111/1541-4337.12006
41. Chávez-González, M. L., Rodríguez-Herrera, R. & Aguilar, C. N. 'Essential oils', in Antibiotic Resistance, Elsevier, 227–237. doi: https://doi.org/10.1016/B978-0-12-803642-6.00011-3. (2016).
42. Jawaid, T. et al. Feb., 'Preparation and Evaluation of Nanoemulsion of Citronella Essential Oil with Improved Antimicrobial and Anti-Cancer Properties', *Antibiotics*, vol. 12, no. 3, p. 478, (2023). https://doi.org/10.3390/antibiotics12030478
43. Szram, A. Mechanical properties of composite material modified with essential oil. *Mater. Eng.* **1** (2), 49–53. https://doi.org/10.15199/28.2017.2.8 (Apr. 2017).
44. Syafiq, R. et al. Oct., 'Antimicrobial Activities of Starch-Based Biopolymers and Biocomposites Incorporated with Plant Essential Oils: A Review', *Polymers*, vol. 12, no. 10, p. 2403, (2020). https://doi.org/10.3390/polym12102403
45. Bonilla, J., Atarés, L., Vargas, M. & Chiralt, A. 'Effect of essential oils and homogenization conditions on properties of chitosan-based films', *Food Hydrocolloids*, vol. 26, no. 1, pp. 9–16, Jan. (2012). https://doi.org/10.1016/j.foodhyd.2011.03.015
46. Husain, A. & Khanam, A. Phycocyanin: a potent bioactive compound. *J. Adv. Res. Sci. Social Sci.* **01** (01), 16 (2019).
47. Li, Y. et al. Sep., 'Progress of Microencapsulated Phycocyanin in Food and Pharma Industries: A Review', *Molecules*, vol. 27, no. 18, p. 5854, (2022). https://doi.org/10.3390/molecules27185854
48. García, A. B., Longo, E. & Bermejo, R. The application of a phycocyanin extract obtained from Arthrospira platensis as a blue natural colorant in beverages. *J. Appl. Phycol.* **33** (5), 3059–3070. https://doi.org/10.1007/s10811-021-02522-z (Oct. 2021).
49. Aliotta, L., Canesi, I. & Lazzeri, A. Study on the Preferential distribution of acetyl tributyl citrate in poly(lactic) acid-poly(butylene adipate-co-terephthalate) blends. *Polym. Test.* **98**, 107163. https://doi.org/10.1016/j.polymertesting.2021.107163 (Jun. 2021).
50. Tian, J. et al. Jun., 'Improving tensile strength and impact toughness of plasticized poly(lactic acid) biocomposites by incorporating nanofibrillated cellulose', *Nanotechnology Reviews*, vol. 11, no. 1, pp. 2469–2482, (2022). https://doi.org/10.1515/ntrev-2022-0142
51. Tsou, C. H. et al. Aug., 'Preparation and Characterization of Bioplastic-Based Green Renewable Composites from Tapioca with Acetyl Tributyl Citrate as a Plasticizer', *Materials*, vol. 7, no. 8, pp. 5617–5632, (2014). https://doi.org/10.3390/ma7085617
52. Brdlík, P., Borůvka, M., Běhálek, L. & Lenfeld, P. 'The Influence of Additives and Environment on Biodegradation of PHBV Biocomposites', *Polymers*, vol. 14, no. 4, p. 838, Feb. (2022). https://doi.org/10.3390/polym14040838
53. Aouachria, K., Massardier, V., Benaniba, M. T. & Belhaneche-Bensemra, N. Evaluation of the effects of acetyl tributyl citrate as bio-based plasticizer on the physical, thermal, and dynamical mechanical properties of poly(vinyl chloride)/polymethyl methacrylate blends. *Vinyl Additive Technol.* **25, no. S1**, https://doi.org/10.1002/vnl.21646 (Jan. 2019).
54. Grigora, M. E., Terzopoulou, Z., Tsongas, K., Bikiaris, D. N. & Tzetzis, D. 'Physicochemical Characterization and Finite Element Analysis-Assisted Mechanical Behavior of Polylactic Acid-Montmorillonite 3D Printed Nanocomposites', *Nanomaterials*, vol. 12, no. 15, p. 2641, Jul. (2022). https://doi.org/10.3390/nano12152641
55. Muniyasamy, S., Ofosu, O., John, M. J. & Anandjiwala, R. D. 'Mineralization of Poly(lactic acid) (PLA), Poly(3-hydroxybutyrate-co-valerate) (PHBV) and PLA/PHBV Blend in Compost and Soil Environments', *j renew mater*, vol. 4, no. 2, pp. 133–145, Apr. (2016). https://doi.org/10.7569/JRM.2016.634104
56. Chieng, B., Ibrahim, N., Yunus, W. & Hussein, M. 'Poly(lactic acid)/Poly(ethylene glycol) Polymer Nanocomposites: Effects of Graphene Nanoplatelets', *Polymers*, vol. 6, no. 1, pp. 93–104, Dec. (2013). https://doi.org/10.3390/polym6010093
57. Mitchell, G. R. 'X ray Scattering from Non Crystalline and Liquid Crystalline Polymers in Comprehensive Polymer Science', G.Allen and J.Bevington Pergamon Press., vol. 1 Chap. 31, pp. 687–729.
58. Gkourmpis, T. & Mitchell, G. R. 'The Use of Scattering Data in the Study of the Molecular Organisation of Polymers in the Non-Crystalline State', *Polymers*, vol. 12, no. 12, p. 2917, Dec. (2020). https://doi.org/10.3390/polym12122917
59. Ma, B. et al. Effect of poly(lactic acid) crystallization on its mechanical and heat resistance performances. *Polymer* **212**, 123–280. https://doi.org/10.1016/j.polymer.2020.123280 (Jan. 2021).
60. Saeidlou, S., Huneault, M. A., Li, H. & Park, C. B. Poly(lactic acid) crystallization. *Prog. Polym. Sci.* **37** (12), 1657–1677. https://doi.org/10.1016/j.progpolymsci.2012.07.005 (Dec. 2012).
61. Langford, A., Chan, C. M., Pratt, S., Garvey, C. J. & Laycock, B. The morphology of crystallisation of PHBV/PHBV copolymer blends. *Eur. Polymer J.* **112**, 104–119. https://doi.org/10.1016/j.eurpolymj.2018.12.022 (Mar. 2019).
62. Hedrick, M. M., Wu, F., Mohanty, A. K. & Misra, M. Morphology and performance relationship studies on biodegradable ternary blends of poly(3-hydroxybutyrate- *Co* -3-hydroxyvalerate), polylactic acid, and polypropylene carbonate. *RSC Adv.* **10** (73), 44624–44632. https://doi.org/10.1039/D0RA07485C (2020).
63. Diab, M. A., El-Sonbati, A. Z., Al-Halawany, M. M. & Bader, D. M. D. 'Thermal Stability and Degradation of Chitosan Modified by Cinnamic Acid', *OJPChem*, vol. 02, no. 01, pp. 14–20, (2012). https://doi.org/10.4236/ojpchem.2012.21003
64. Blázquez-Blázquez, E., Barranco-García, R., Díez-Rodríguez, T. M., Cerrada, M. L. & Pérez, E. 'Combined Effects from Dual Incorporation of ATBC as Plasticizer and Mesoporous MCM-41 as Nucleating Agent on the PLA Isothermal Crystallization in Environmentally-Friendly Ternary Composite Systems', *Polymers*, vol. 15, no. 3, p. 624, Jan. (2023). https://doi.org/10.3390/polym15030624
65. Zhang, W. et al. Effects of heating rate on thermal degradation behavior and kinetics of representative thermoplastic wastes. *J. Environ. Manage.* **314**, 115071. https://doi.org/10.1016/j.jenvman.2022.115071 (Jul. 2022).
66. Niu, M., Zhang, Z., Wei, Z. & Wang, W. Effect of a novel flame retardant on the mechanical, thermal and combustion properties of Poly(Lactic Acid). *Polymers* **12** (10), 2407. https://doi.org/10.3390/polym12102407 (Oct. 2020).
67. Oyama, I. M. C., Dos Anjos, E. G. R., De Melo Morgado, G. F., Martins, E. F. & Passador, F. R. 'Antistatic and antimicrobial packaging of PLA / PHBV blend-based graphene nanoplatelets nanocomposites', *J of Applied Polymer Sci*, vol. 140, no. 40, pp. 1–17, Oct. (2023). https://doi.org/10.1002/app.54484
68. Maiza, M., Benaniba, M. T., Quintard, G. & Massardier-Nageotte, V. 'Biobased additive plasticizing Polylactic acid (PLA)', *Polímeros*, vol. 25, no. 6, pp. 581–590, Dec. (2015). https://doi.org/10.1590/0104-1428.1986
69. Zhang, K., Mohanty, A. K. & Misra, M. 'Fully Biodegradable and Biorenewable Ternary Blends from Polylactide, Poly(3-hydroxybutyrate-co-hydroxyvalerate) and Poly(butylene succinate) with Balanced Properties', *ACS Appl. Mater. Interfaces*, vol. 4, no. 6, pp. 3091–3101, Jun. (2012). https://doi.org/10.1021/am3004522
70. Righetti, M. C., Cinelli, P., Mallegni, N., Stäbler, A. & Lazzeri, A. 'Thermal and Mechanical Properties of Biocomposites Made of Poly(3-hydroxybutyrate-co-3-hydroxyvalerate) and Potato Pulp Powder', *Polymers*, vol. 11, no. 2, p. 308, Feb. (2019). https://doi.org/10.3390/polym11020308
71. Righetti, M. C. et al. Feb., 'Thermal, Mechanical, and Rheological Properties of Biocomposites Made of Poly(lactic acid) and Potato Pulp Powder', *IJMS*, vol. 20, no. 3, p. 675, (2019). https://doi.org/10.3390/ijms20030675
72. Gálvez, J. et al. 'Effect of Extrusion Screw Speed and Plasticizer Proportions on the Rheological, Thermal, Mechanical, Morphological and Superficial Properties of PLA', *Polymers*, vol. 12, no. 9, p. 2111, Sep. (2020). https://doi.org/10.3390/polym12092111
73. Handayani, S. U., Fahrudin, M., Mangestiyono, W., Hadi, A. F. & Muhamad Mechanical properties of commercial recycled polypropylene from plastic waste. *J. Vocat. Stud. Appl. Res.* **3** (1), 1–4. https://doi.org/10.14710/jvsar.v3i1.10868 (May 2021).
74. Callister, W. D. & Rethwisch, D. G. *Fundamentals of materials science and engineering: an integrated approach*, 5th edition, Wiley Binder version. Hoboken: Wiley, (2015).
75. Yuan, Y. & Lee, T. R. 'Contact angle and wetting properties.' In *Surface Science Techniques* Vol. 51 (eds Bracco, G. & Holst, B.) 3–34 (Springer Berlin Heidelberg, 2013). https://doi.org/10.1007/978-3-642-34243-1_1.
76. Galindo, S. & Urena-Nuñez, F. 'Enhanced surface hydrophobicity of poly(lactic acid) by Co^{60} gamma ray irradiation', *Rev. Mex. Fís.*, vol. 64, no. 1 Jan-Feb, pp. 1–7, Oct. (2017). https://doi.org/10.31349/RevMexFis.64.1

77. Shi, J. et al. Dec., 'Crystallinity Dependence of PLLA Hydrophilic Modification during Alkali Hydrolysis', *Polymers*, vol. 15, no. 1, p. 75, (2022). https://doi.org/10.3390/polym15010075
78. Snowdon, M. R., Mohanty, A. K. & Misra, M. Miscibility and performance evaluation of biocomposites made from Polypropylene/Poly(lactic acid)/Poly(hydroxybutyrate- *co* -hydroxyvalerate) with a Sustainable Biocarbon Filler. *ACS Omega*. **2** (10), 6446–6454. https://doi.org/10.1021/acsomega.7b00983 (Oct. 2017).
79. Kołbuk, D., Ciechomska, M., Jeznach, O. & Sajkiewicz, P. Effect of crystallinity and related surface properties on gene expression of primary fibroblasts. *RSC Adv.* **12** (7), 4016–4028. https://doi.org/10.1039/D1RA07237D (2022).
80. Meereboer, K. W., Pal, A. K., Cisneros-López, E. O., Misra, M. & Mohanty, A. K. The effect of natural fillers on the marine biodegradation behaviour of poly(3-hydroxybutyrate-co-3-hydroxyvalerate) (PHBV). *Sci. Rep.* **11** (1), 911. https://doi.org/10.1038/s41598-020-78122-7 (Jan. 2021).
81. Ye, J. R., Chen, L., Zhang, Y., Zhang, Q. C. & Shen, Q. Turning the Chitosan surface from hydrophilic to hydrophobic by layer-by-layer electro-assembly. *RSC Adv.* **4** (102), 58200–58203. https://doi.org/10.1039/C4RA10327K (2014).
82. Kim, H. et al. Oct., 'Pharmacokinetic Properties of Acetyl Tributyl Citrate, a Pharmaceutical Excipient', *Pharmaceutics*, vol. 10, no. 4, p. 177, (2018). https://doi.org/10.3390/pharmaceutics10040177
83. *ISO 527-2 Plastics — Determination of tensile properties Part 2: Test conditions for moulding and extrusion plastics*, (2012).
84. Iacob, D. V., Zisopol, D. G. & Minescu, M. 'Technical-Economical Study on the Optimization of FDM Parameters for the Manufacture of PETG and ASA Parts', *Polymers*, vol. 16, no. 16, p. 2260, Aug. (2024). https://doi.org/10.3390/polym16162260
85. Crump, S. S. 'Apparatus and method for creating three-dimensional objects', 5,121,329, Jun. 09, 1992 Accessed: Feb. 19, 2025. [Online]. Available: https://patents.google.com/patent/US5121329A/en
86. 'BL11 NCD-SWEET. online accessed on 1st August 2024', BEAMLINE INFORMATION — en (cells.es) accessed on 1st August 2024.
87. Gonzalez, N. et al. 'Beam Conditioning Optics at the ALBA NCD-SWEET Beamline', *Mechanical Eng. Design of Synchrotron Radiation Equipment and Instrumentation MEDSI2018, Paris, France*, (2018). https://doi.org/10.18429/JACOW-MEDSI2018-THPH14
88. *ISO 11357-2: Plastics — Differential scanning calorimetry (DSC) —Part 2: Determination of glass transition temperature and glass transition step height*, (2020).
89. *ISO 1133-1:2022 Plastics — Determination of the melt mass-flow rate (MFR) and melt volume-flow rate (MVR) of thermoplastics Part 1: Standard method*, (2022).

Acknowledgements

The work was supported by the funding program RE-C05-i01, EMBALAGEM DO FUTURO, financed by PRR - Plano de Recuperação e Resiliência pela União Europeia (Next Generation EU). The authors also acknowledge the Fundação para a Ciência e a Tecnologia (FCT) through the project PTDC/BTA-GES/2740/2020_NABIA, DOI 10.54499/PTDC/BTA-GES/2740/2020 and the Coimbra Chemistry Centre- Institute of Molecular Sciences (CQC-IMS) supported by the FCT through the project UIDB/00313/2020 and UIDP/00313/2020. The authors acknowledge Fundação para a Ciência e a Tecnologia (FCT) for its financial support via the project CDRSP Base Funding (DOI: 10.54499/UIDB/04044/2020); PRR 2375 Bioshoes4All and PRR INOVAM C644865234-00000004. The work of the GRM was supported in part by Visionary Equation lda. The experiments at the ALBA Synchrotron Light Source in Barcelona were performed in collaboration with ALBA staff. We are grateful to Skingreen for contributing to the packaging design and to Kitosano for kindly supplying the CS used in this investigation. The authors would like to thank Diana Pacheco, Marta Lourenço, Miguel Silva, and Alexandre Gomes for their assistance in the SEM experiments and Joana Valente and Tatiana Patricio for supervising them. We would also like to thank Rosane Silva and Ricardo Lopes for their assistance in the additive manufacturing experiments.

Author contributions

Conceptualization: TE; Data Curation: FS, PR, PV, AMassano, GM and CB; Formal analysis: FS, PR, AMateus, GM, AS and TE; Funding acquisition: TE, AMateus, GM and AS; Investigation: FS, AMassano, GM, AS, TE and AMateus; Methodology: FS, PR, PV, AMateus, AMassano, CB, VC, GM and TE; Project administration: TE; Resources: TE, AS, AMateus and LMO; Supervision: TE, AS and AMateus; Validation: TE, AS and AMateus; Visualization: All authors; Roles/Writing- original draft: FS, PR, AMassano, GM, AMateus, AS and TE; Writing-review and editing: FS, AS and TE.

Funding

The work was supported by the funding program RE-C05-i01, EMBALAGEM DO FUTURO, financed by PRR - Plano de Recuperação e Resiliência pela União Europeia (Next Generation EU).

Declarations

Competing interests

Authors Telma Encarnação and Fátima Santos were employed by PTScience. Luís Miguel Oliveira was employed by AMCubed. Geoffrey R. Mitchell employed by Visionary Equation Lda. The remaining authors declare that the research was conducted in the absence of any commercial or financial relationships that could be construed as potential conflicts of interest.

Additional information

Supplementary Information The online version contains supplementary material available at https://doi.org/10.1038/s41598-025-10426-y.

Correspondence and requests for materials should be addressed to F.S. or T.E.